Local Measurements of Viscoelastic Parameters of Adherent Cell Surfaces by Magnetic Bead Microrheometry

Andreas R. Bausch,* Florian Ziemann,* Alexei A. Boulbitch,* Ken Jacobson,[#] and Erich Sackmann*

*Physik Department E22 (Biophysics Group), Technische Universität München, D-85748 Garching, Germany, and [#]Department of Cell Biology and Anatomy, University of North Carolina, Chapel Hill, North Carolina 27599-7090 USA

ABSTRACT   A magnetic bead microrheometer has been designed which allows the generation of forces up to 10^4 pN on 4.5 μm paramagnetic beads. It is applied to measure local viscoelastic properties of the surface of adhering fibroblasts. Creep response and relaxation curves evoked by tangential force pulses of 500-2500 pN (and ~1 s duration) on the magnetic beads fixed to the integrin receptors of the cell membrane are recorded by particle tracking. Linear three-phasic creep responses consisting of an elastic deflection, a stress relaxation, and a viscous flow are established. The viscoelastic response curves are analyzed in terms of a series arrangement of a dashpot and a Voigt body, which allows characterization of the viscoelastic behavior of the adhering cell surface in terms of three parameters: an effective elastic constant, a viscosity, and a relaxation time. The displacement field generated by the local tangential forces on the cell surface is visualized by observing the induced motion of assemblies of nonmagnetic colloidal probes fixed to the membrane. It is found that the displacement field decays rapidly with the distance from the magnetic bead. A cutoff radius of $R_c \sim 7$ μm of the screened elastic field is established. Partial penetration of the shear field into the cytoplasm is established by observing the induced deflection of intracellular compartments. The cell membrane was modeled as a thin elastic plate of shear modulus μ^* coupled to a viscoelastic layer, which is fixed to a solid support on the opposite side; the former accounts for the membrane/actin cortex, and the latter for the contribution of the cytoskeleton to the deformation of the cell envelope. It is characterized by the coupling constant χ characterizing the elasticity of the cytoskeleton. The coupling constant χ and the surface shear modulus μ^* are obtained from the measured displacements of the magnetic and nonmagnetic beads. By analyzing the experimental data in terms of this model a surface shear modulus of $\mu^* \approx 2 \cdot 10^{-3}$ Pa m to $4 \cdot 10^{-3}$ Pa m is found. By assuming an approximate plate thickness of 0.1 μm one estimates an average bulk shear modulus of $\mu \approx (2 \div 4) \cdot 10^{-4}$ Pa, which is in reasonable agreement with data obtained by atomic force microscopy. The viscosity of the dashpot is related to the apparent viscosity of the cytoplasm, which is obtained by assuming that the top membrane is coupled to the bottom (fixed) membrane by a viscous medium. By application of the theory of diffusion of membrane proteins in supported membranes we find a coefficient of friction of $b_c \approx 2 \cdot 10^9$ Pa s/m corresponding to a cytoplasmic viscosity of $2 \cdot 10^3$ Pa s.

INTRODUCTION

Viscoelasticity plays an important role in the behavior of cells. It is a key factor in the regulation of the cell shape of resting and moving cells, and it has even been conjectured that the viscoelastic coupling between the plasma membrane and the cell nucleus plays a role in the control of genetic expression (Ingber, 1997; Forgacs, 1996). The cell viscoelasticity is determined in a complex way by the composite shell envelope composed of the lipid-protein bilayer with the associated actin cortex and by the internal cytoskeleton composed of actin microfilaments, microtubules, intermediate filaments, and their associated proteins. High-precision measurements of viscoelastic parameters of cells are thus expected to give insight into the structure of the cortical and internal cytoskeleton. Moreover, such measurements

are of great practical value in order to quantify the effect of drugs, mutations, or diseases on the cell structure. Viscoelastic measuring techniques must fulfill three conditions. First, they must allow local measurements on micrometer-to-nanometer scales to account for the inherent heterogeneous architecture of cell envelopes. Since cellular deformations may be followed by biochemically induced changes of the local viscoelastic parameters, the techniques must secondly allow repeated measurements. To compare the data, the third requirement is that the data analysis is independent of a specific cell model. These requirements are fulfilled by microrheological techniques based on optical tweezers (Choquet et al., 1997), atomic force microscopy (Radmacher et al., 1996), magnetic bead rheometry (Ziemann et al., 1994), and cell poking elastometer (Pasternak et al., 1995). An intriguing magnetic particle technique used to assay the cytoplasmic viscosity and intracellular mobilities has been developed by Valberg et al. (cf. Valberg and Feldman, 1987). It is based on the analysis of the decay of remnant magnetic fields after twisting the magnetic particles. It corresponds to our relaxation response analysis. The major differences of this technique as compared to the others is that many particles distributed within the cell are monitored. Moreover, the method yields average values of the cytoplasmic viscosities.

Another strategy used to measure local elastic properties was established recently. It is based on the analysis of the surface profile of adhering cells near the contact area and its alteration by viscous shear forces in terms of the elastic boundary (Simson et al., 1998).

Many cell types such as *Dictyostelium* cells, white blood cells, fibroblasts, or endothelial cells exhibit elastic moduli of the order of 10^3 to 10^4 Pa and forces in the nanonewton regime are required for the deformation of these cells (cf. Evans, 1995; Radmacher et al., 1996). For this purpose, we developed a magnetic bead microrheometer ("magnetic tweezers") allowing application of local forces of up to 10 nN on paramagnetic beads of 4.5 μm diameter. This technique is applied to measure viscoelastic parameters of the cell envelope of fibroblasts adhering to solid substrates.

Magnetic beads (of 4.5 μm diameter) coated with fibronectin are fixed to integrin receptors of the cell surface. Creep response and relaxation curves evoked by tangential force pulses of 500-2500 pN (and ~1 s duration) are determined by the particle tracking technique. A linear viscoelastic response is found for forces up to 2 nN in contrast to the increase of local stiffness with stress amplitude reported by Ingber (1997).

Three-phasic creep response curves exhibiting an elastic domain, a relaxation regime, and viscous flow behavior are found. This three-phasic response is formally accounted for by a mechanical equivalent circuit consisting of a Voigt body and a dashpot in series where the Voigt element (composed of a Maxwell body and a spring in parallel arrangement) accounts for the solidlike and the dashpot for the fluidlike behavior. Based on the above analysis the viscoelastic behavior of the cell is characterized by three parameters: an elastic constant (k), a relaxation time (τ), and a viscosity (γ_0).

To relate these parameters to viscoelastic moduli of the cell envelope and the cytoplasm, the adhering cell lobe is modeled by a thin elastic plate which is coupled to a viscoelastic layer fixed on the side opposite to the substrate. The elasticity of the top plate (representing the plasma membrane) is characterized by a surface shear modulus μ^*. It is related to the shear modulus μ of the material as $\mu^* = \mu h$, where h is the thickness of the shell composed of the membrane and actin cortex. The elastic effect of the intermediate layer is characterized by a phenomenological coupling constant χ, referred to as the cytoskeleton coupling constant.

According to a theory of A. Boulbitch (1998, submitted for publication; cf. Appendix for summary) the displacement field generated by a local tangential force on the top membrane exhibits a logarithmic behavior in the plane of the membrane at distances r much smaller than a screening length R_c while it decays exponentially at $r \gg R_c$. The screening length R_c is related to the shear modulus μ^* and the coupling constant χ by $R_c = \kappa^{-1} = (\mu^*/\chi)^{1/2}$.

Experimental evidence for such a screened elastic deformation of the cell surface is provided by accompanying displacement field mapping experiments (Schmidt et al.,

1996). The local displacement of the membrane surface evoked by the local tangential force is directly visualized by observing the induced motion of colloidal probe beads attached to the cell membrane in the neighborhood of the magnetic bead. It is demonstrated that the displacement field decays rapidly with a cutoff radius of $R_c \approx 7$ μm. By analyzing the observed decay of the displacement field with the distance from the magnetic bead in terms of the theoretical model, one obtains values of χ and μ^*. It is thus possible to relate the elastic constant (k) obtained from the equivalent circuit analysis to an absolute shear modulus of the cell envelope.

For the evaluation of the viscous flow regime it is assumed that the top membrane of the adhering cell lobe is coupled to the bottom (fixed) membrane by a viscous fluid. The apparent viscosity of this fluid is obtained from the velocity of the magnetic bead by application of a theory previously elaborated to describe the diffusion of proteins embedded in a bilayer membrane coupled to a solid surface through a thin lubricating film (Evans and Sackmann, 1988). This theory predicts that the viscous flow field in the membrane is again screened by this frictional coupling (Evans and Sackmann, 1988). Thus the viscosity of the cytoplasm can also be related to the value of the viscosity of the dashpot γ_0. The screened penetration of the shear field into the cytoplasm was observed by the induced deflection of intracellular compartments.
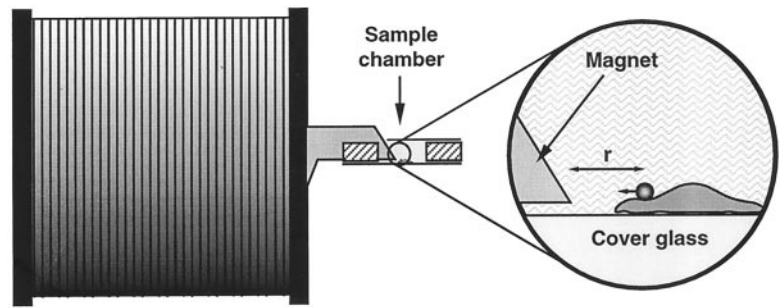
MATERIALS AND METHODS

The high force magnetic bead rheometer

The microrheometer resembles the experimental set-up described previously (Ziemann et al., 1994; Schmidt et al., 1996). It consists of a central measuring unit comprised of a sample holder and a magnetic coil with 1200 turns of 0.7 mm copper wire. The sample holder with dimension $50 \times 55 \times 50$ mm^3 is mounted on an AXIOVERT 10 microscope (Zeiss, Oberkochen, Germany). The coil current is produced by a voltage-controlled current supply built in the authors' laboratory that transforms the voltage signal of a function generator FG 9000 (ELV, Leer, Germany) in a current signal with amplitudes of up to 4 A. The microscope image is recorded by a CCD camera (C3077, Hamamatsu Photonics, Hamamatsu City, Japan) connected to a VCR (WJ-MX30, Matsushita Electric Industrial Co., Osaka, Japan). The recorded sequences are digitized using an Apple Power Macintosh 9500 (Apple Computer, Cupertino, CA) equipped with a LG3 frame grabber card (Scion Corp., Frederick, MD). The position of the particles is determined with an accuracy of ~10 nm using a self-written single particle tracking algorithm implemented in the public domain image processing software National Institutes of Health Image (National Institutes of Health, Bethesda, MD).

The important modification of the present apparatus, compared to the previous one, is that only one magnetic coil is used in which the edge of the pole piece can be positioned as close as 10 μm from the magnetic particle (see Fig. 1). Because of the very high field gradient in the close vicinity of the pole piece, forces could be increased by a factor of ~10^3 compared to the earlier design (Ziemann et al., 1994). Thus, forces of up to 10 nN on a 4.5-μm paramagnetic bead were achieved (cf. Fig. 2). By using ferromagnetic beads such forces could be achieved with bead diameters of 0.5 μm. A second magnet cannot be used in the present device because of the strong magnetic induction generated between the pole pieces at such small distances.

FIGURE 1   Central measuring unit of the improved magnetic bead rheometer set-up. The magnet consists of a coil (1200 turns of 0.7 mm copper wire) and a soft iron core, which penetrates the sample chamber. The coil is fixed with a holder that can be placed on the microscope stage. The tip of the pole piece can be positioned close to the magnetic bead (at distances of $r = 10–100$ μm) to obtain maximal forces of up to 10,000 pN on a 4.5-μm paramagnetic bead.

Force calibration of the set-up

To calibrate the distance dependence of the force acting on the magnetic bead in the high force set-up, the bead velocity was determined near the pole piece in liquids of known viscosity at different coil currents ranging from 250 to 2500 mA. The bead velocity was computed from the measured displacement-time-graphs by numerical differentiation. Fig. 2 shows the results of a typical calibration of the force on a 4.5-μm paramagnetic bead (DYNABEADS M-450, Dynal, Oslo, Norway). We used dimethyl-polysiloxane with a kinematic viscosity of 12,500 cSt (DMPS-12M, Sigma Chemical Company, St. Louis, MO) as a calibrating liquid.

The velocity curves were converted into force curves using Stokes law and plotted versus the distance to the pole piece (see Fig. 2 *a*). For the highest coil currents, forces of up to 10,000 pN on a 4.5-μm paramagnetic bead were reached. The curves shown in Fig. 2 *a* were all obtained by using the same bead. For each measurement the bead was aspirated by a micropipette and pulled back to its starting position (at a distance of 110 μm to the pole piece). Thus, the errors resulting from different bead sizes and iron contents ($\sim$15–20%) could be avoided.

In Fig. 2 *b* the magnetic force is plotted versus the coil current for different distances from the pole piece. This graph shows a linear dependence between force and current indicating that the paramagnetic bead is fully magnetized and therefore does not exhibit a field-dependent magnetic moment, which would be the case for paramagnetic particles in low magnetic fields.

The overall error of the method for measuring absolute forces is determined by the standard deviations of the bead size and the iron content and was estimated to 15–20%. For relative measurements (performed with the same bead), the overall error depends only on the accuracy of the determination of the bead velocity and of the coil current. This leads to a small total error for relative measurements of forces and viscoelastic constants of 1–2%.

Sample preparation

The rheological measurements presented here were performed on National Institutes of Health 3T3 murine fibroblasts employing paramagnetic mi-crobeads of 4.5 μm diameter bound to the cell membrane. National Institutes of Health 3T3 cells were provided by the Max-Planck-Institut für Zellbiologie (Martinsried, Germany). The cells were cultured in an incubator at 37°C and 5% CO_2. The cell culture medium consisted of DMEM with 10% v/v fetal calf serum (both from Life Technologies, Frederick, MD).
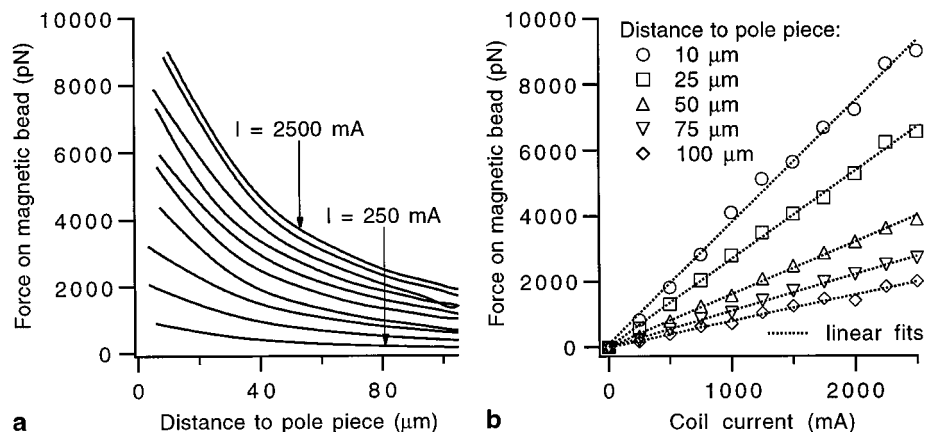
As shown in Fig. 3, the microbeads were coated with fibronectin, which provides indirect coupling to the actin cortex via integrins located in the cell membrane (Miyamoto et al., 1995; Wang et al., 1993). Fibronectin was covalently conjugated to 4.5-μm diameter paramagnetic polystyrene beads coated with reactive tosyl groups (DYNABEADS M-450 tosylactivated, Dynal) according to the procedure provided by the supplier. Carboxylated latex beads with a diameter of 1 μm (POLYBEADS, Polysciences, Warrington, PA) were used as nonmagnetic colloidal probes for the visualization of the displacement field on the cell membrane (cf. Fig. 8). These beads were also coated with fibronectin to ensure the coupling to the integrins.

Immediately before sample preparation the functionalized magnetic beads were washed once in PBS (phosphate buffered saline, Sigma Chemical Co.) using a magnetic separation device (MPC-1, Dynal) and the bead concentration was adjusted to $\sim$10^5 beads/ml. Cells were then detached from the substratum using a trypsin-EDTA solution (Life Technologies) and transferred onto suitable coverglasses. After an incubation time of 1–2 h to allow complete adhesion of the cells, 1.5 ml bead solution per coverglass was added. Beads were incubated with cells for 15 min and washed gently before mounting the coverglass on the sample holder of the magnetic bead rheometer.

Evaluation of creep experiments by mechanical equivalent circuit

Creep experiments are performed by recording the deflection and relaxation of the magnetic beads (or nonmagnetic probe beads) following rectangular force pulses. The trajectories of the beads are determined by the single particle tracking technique with an accuracy of ±10 nm. Fig. 4 shows a typical sequence of responses of a magnetic bead to a sequence of

FIGURE 2   Force calibration of a 4.5-μm magnetic bead for the high force set-up. (*a*) Distance dependence of the force on the bead for 10 different coil currents (250–2500 mA). (*b*) Force-versus-current curves for the five distances indicated in the inset showing a linear relationship between the coil current and the force on the (fully magnetized) paramagnetic bead.
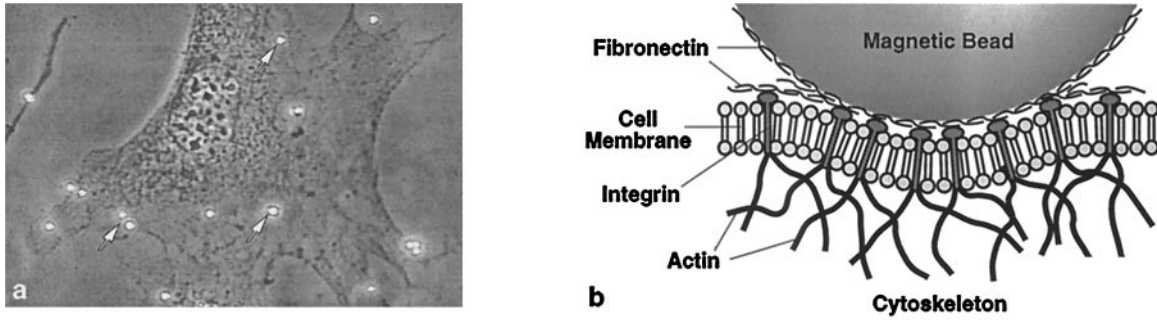
FIGURE 3   (*a*) Micrograph of a mouse 3T3 fibroblast with magnetic microbeads bound to the cell membrane (*white arrows*). (*b*) Schematic drawing of a fibronectin-coated bead that is coupled to the cell cytoskeleton via integrins.

rectangular force pulses of duration $\Delta t = 2.5$ s. The responses exhibit three regimes: a fast elastic response (I), a relaxation regime (II), and a flow regime (III).

The time-dependent deflection $x(t)$ of the body of Fig. 5 *a* evoked by a stepwise force $F(t)$ can be easily expressed as superposition of the deflection of the Voigt body and of the dashpot according to Fung (1993). Therefore, the deflection of the bead (normalized by the applied force amplitude F) is given by

$$\frac{x(t)}{F} = \frac{1}{k_0}\left(1 - \frac{k_1}{k_0 + k_1} \cdot \exp(-t/\tau)\right) + \frac{t}{\gamma_0}, \qquad (1a)$$

where the relaxation time τ is given by

$$\tau = \frac{\gamma_1(k_0 + k_1)}{k_0 k_1}. \qquad (1b)$$

The characteristic time behavior of the equivalent circuit is shown in Fig. 5 *b* and the similarity with the sequence of response and relaxation curves in Fig. 4 is evident. As shown in Fig. 6 the creep response curves are very well reproduced by Eq. 1a.

The four parameters characterizing the equivalent circuit can be reduced to three observables with the following physical meaning: because the amplitude of the elastic displacement (regime I) is determined by $x = F/(k_0 + k_1)$ the sum $k = k_0 + k_1$ is a measure of the effective spring constant of the system. As defined in Eq. 1b, τ is the relaxation time required for the transition from the elastic to the viscous regime and γ_0 is a measure for the effective viscous friction coefficient of the bead in the viscous flow regime.

The analysis of the viscoelastic response curves evoked by the tangential force pulses in terms of the three observables defined above is a first and straightforward step of data analysis. It is sufficient to observe local variations of the viscoelastic properties on the cell surface or to study differences between different cells (cf. Fig. 7). However, it is a much more
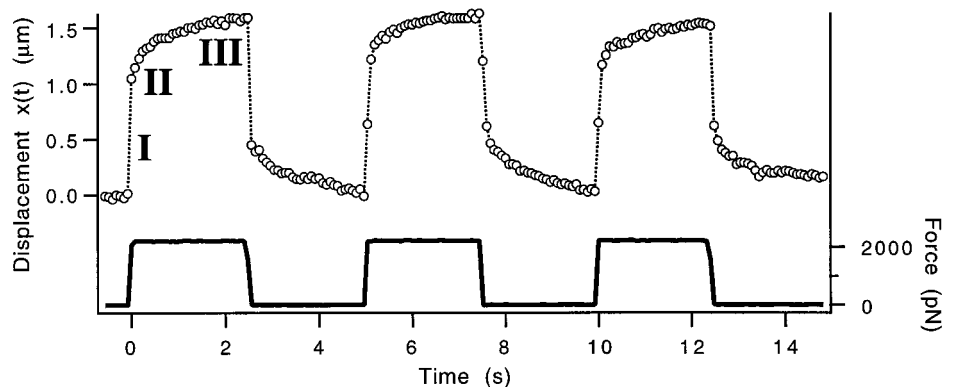
difficult task to relate these parameters to viscoelastic moduli of the cell surface or the cytoplasm. This will be attempted below by introduction of a simplified model of the adhering cell lobes.

RESULTS AND DISCUSSION

Evaluation of response curve in terms of equivalent circuit

We studied the creep response curves of 10 cells while analyzing several magnetic beads on each cell. Moreover, measurements were performed for three to five different traction forces for each magnetic bead. The three viscoelastic parameters k, τ, and γ_0 defined above (cf. Eqs. 1) were determined by analysis of the creep-response curves as described in Fig. 5. The data are summarized in Fig. 7. To distinguish the results obtained for different cells or on different sites on the adhering lobe of one cell the individual measurements are plotted separately. Values for different cells are distinguished by different symbols. Open and closed symbols of the same shape characterize measurements of the same cell but at different sites. Measurements performed with the same particle but with different force amplitudes are marked with equal symbols. A closer inspection of the data shows that all viscoelastic parameters may differ by up to an order of magnitude from cell to cell, but that the values obtained for each individual cell differ by much less.

FIGURE 4   Typical creep response and relaxation curves observed for a 4.5-μm bead bound to the membrane of a 3T3 fibroblast through a presumed fibronectin-integrin linkage. Force pulses of an amplitude of $F = 2000$ pN and a duration of $\Delta t = 2.5$ s were applied.
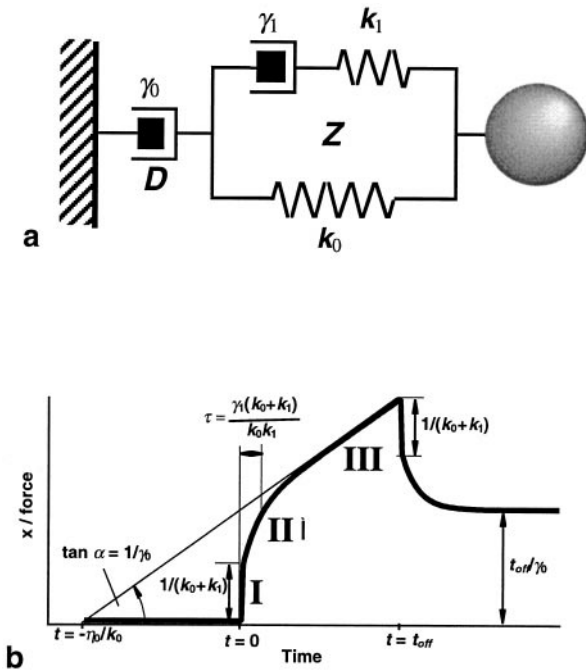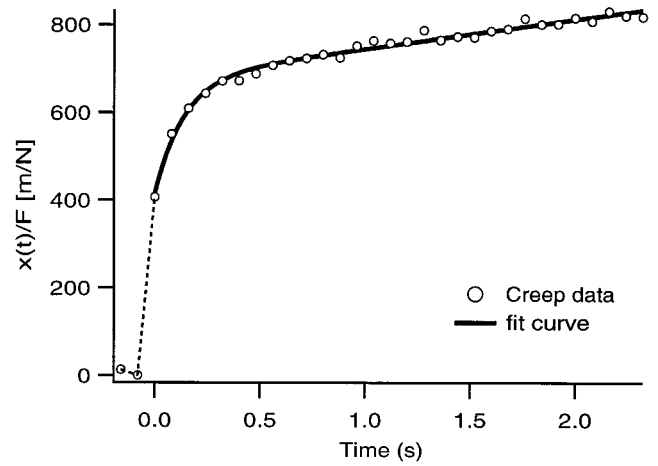
FIGURE 6   Typical fit to measured creep data for a force of $F = 1100$ pN. The dotted line represents the instantaneous elastic response of the magnetic bead corresponding to a jump in the displacement of $1/(k_0 + k_1)$.

FIGURE 5   Mechanical equivalent circuit enabling formal representation of creep response and relaxation curves. (*a*) Mechanical model consisting of a *Kelvin* (or *Zener*) body (*Z*) and a dashpot (*D*) in series. (*b*) Creep response and relaxation curve of the mechanical equivalent circuit exhibiting the three experimentally observed regimes of response (I–III).

To check the linearity of the viscoelastic response, the creep response curves were recorded as a function of the applied forces ranging from 500 to 2000 pN. In Fig. 8 the time-dependence of the displacements (normalized by the applied force) obtained for different applied forces is plotted. In this example the curves coincide within experimental error with the exception of the curve for $F = 2213$ pN. This implies that the viscoelastic behavior of the system is linear for at least forces of up to ~2000 pN. The measurements of the viscoelastic moduli presented in Fig. 7 were performed in the linear regime using forces up to 2000 pN.

Strain field mapping experiment

A typical experiment is shown in Fig. 9. A number of nonmagnetic colloidal latex beads (numbered 1 to 9) are deposited on the cell surface together with one magnetic bead (marked as M). Beads are bound to integrins via the fibronectin coating. The creep response and relaxation curves generated by rectangular force pulses of 3700 pN were recorded by using the particle tracking technique. The amplitudes of deflection generated by pulses of 1 s duration normalized with respect to the polar angle cos θ (cf. Eq. 2 below) were measured and plotted in Fig. 9 *c*. Although the relaxation time τ is of the order of 0.1 s we use the amplitudes at $t = 1$ s as a measure for the elastic displacement. Because all creep response curves exhibit essentially the same shape, this approximation procedure is justified. These measurements were also performed at a force larger

than 2000 pN to facilitate the observation of the particle deflections. However, several displacement field mapping experiments performed with lower forces yielded the same distance-dependence of the normalized deflections.
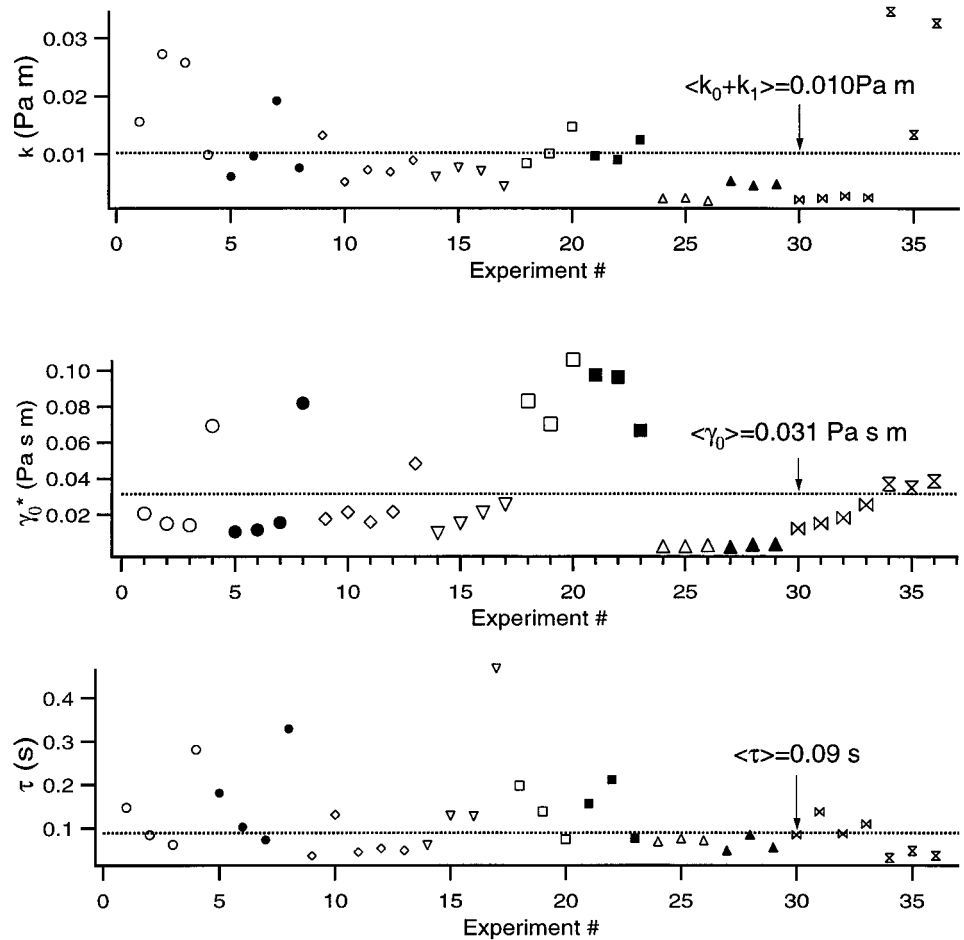
The three nonnumbered beads in Fig. 9 were also deflected, but the deflection amplitude could not be measured accurately enough since the images overlap, thus preventing the application of the particle tracking procedure. Another intriguing way to determine the displacement field is the use of intracellular particles as markers instead of latex particles. In Fig. 10 an experiment is presented demonstrating that cell vacuoles exhibit detectable induced deflection amplitudes (see bottom row in Fig. 10 *b*). The experiment shows that the shear displacement field penetrates partially into the cell cytoplasm; thus intracellular particles may potentially be used as probes to estimate the local penetration depth of the displacement field.

Evaluation of the displacement field data by a simple cell model

To determine real elastic moduli (and shear viscosities) of the cell envelope from the viscoelastic parameters obtained by analyzing the creep response curves in terms of the equivalent circuit, one requires a theory of the elastic displacement of the adhering cell lobe generated by local tangential forces acting on the cell surface. Such models yield the geometric prefactor relating the elastic modulus of the cell surface to the spring constant of the equivalent circuit.

Because the microscopic structure of the cell lobe is not known, one has to introduce suitable models. One obvious possibility would be to consider the cell lobe as a thin homogeneous elastic slab, one side of which is fixed to a solid surface. However, this model would not account for the fact that the cell lobe is composed of two juxtaposed

FIGURE 7 Summary of three pertinent viscoelastic parameters of 3T3 fibroblasts: the effective elastic modulus $k = k_0 + k_1$, the viscosity γ_0, and the relaxation time τ (defined by Eq. 1b) are obtained by analyzing the creep response curves in terms of the equivalent circuit. To distinguish the results obtained for different cells or on different sites on the adhering lobe of one cell, the individual measurements are plotted separately. Values for different cells are distinguished by different symbols. Open and closed symbols of the same shape characterize measurements of the same cell but at different sites. Measurements performed with the same particle but with different force amplitudes are marked with equal symbols.

membranes and that these are interconnected by an intracellular cytoskeleton, as follows from the distribution of intracellular compartments in the cell lobe.
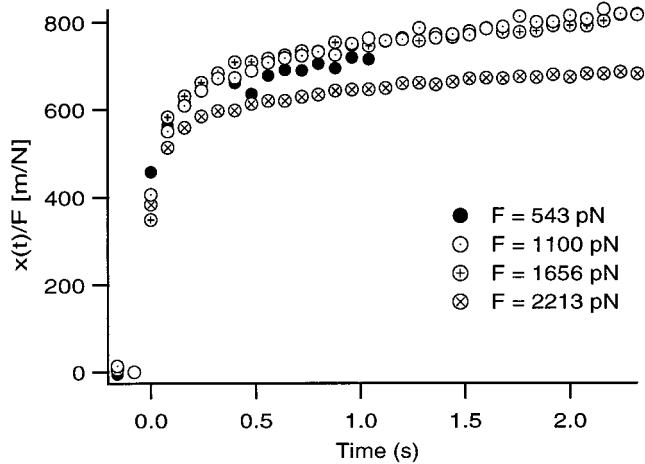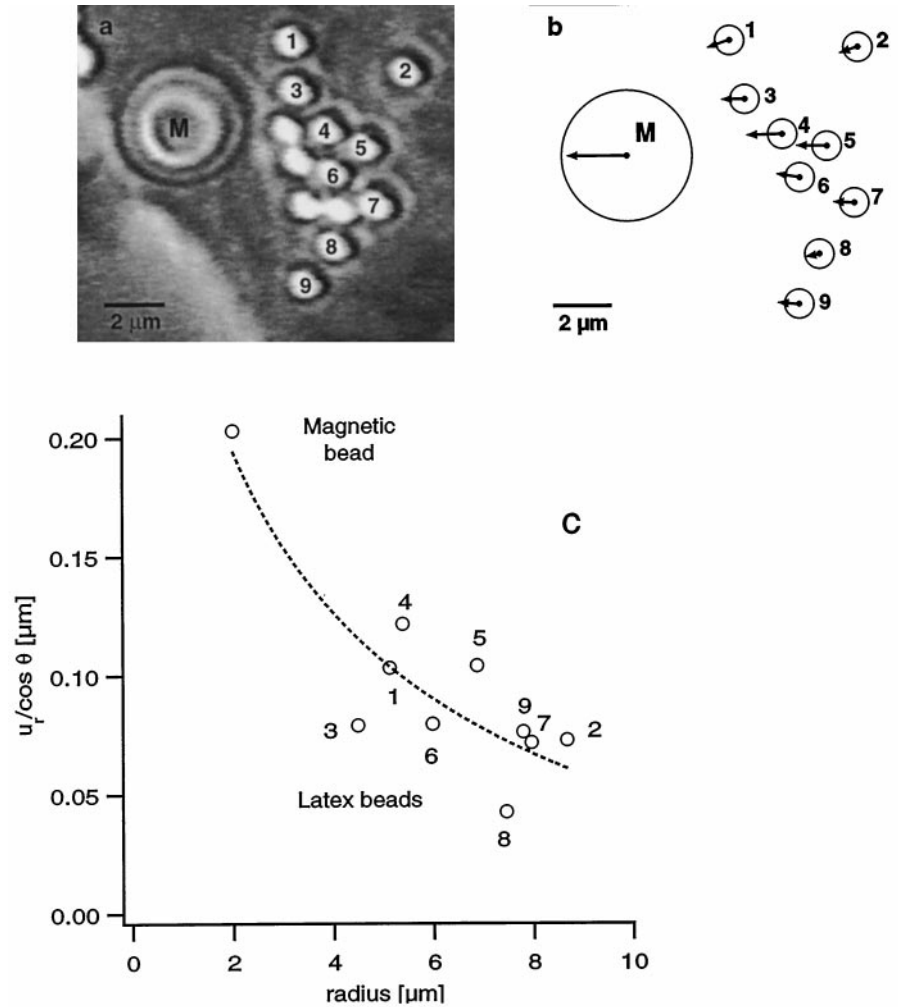

FIGURE 8 Time dependence of the deflection of the magnetic bead normalized with respect to the force for four different forces indicated, demonstrating linear viscoelasticity up to forces of at least 2000 pN. The maximum displacement is $u(r) = 1$ μm for the maximum force of 2000 pN. Most measurements were performed at 500-1000 pN. The maximal value of the strain tensor component was 5%.

In view of these considerations, we assume that the cell lobe can be considered as a partially collapsed shell composed of a lipid-protein bilayer with associated actin cortex (called the composite plasma membrane), and which is filled by a viscoelastic gel coupled to the actin cortex. Therefore the adhering cell lobe is mimicked as two juxtaposed elastic sheets of shear modulus μ^* (representing the composite membrane), which are attached to an elastic medium (accounting for the cytoskeleton). The coupling between the actin cortex and the cytoskeleton is characterized by a phenomenological coupling constant χ, which is a measure for the cytoskeleton membrane coupling strength per unit area (see the Appendix for details). It is further assumed that the bottom shell is fixed to the surface and it is not deformed during our measurements. This assumption is justified by the fact that the displacement field decays rapidly within the cytoplasm (cf. Fig. 9).

The problem of the elastic deformation of such a body by a tangential point force acting on the surface has been solved by A. Boulbitch (1998, submitted for publication). The essential results are summarized in the Appendix where the general expression for the displacement field is given. The main result is that the displacement field $\mathbf{u}(r, \theta)$ caused by the local force is screened. It depends logarithmically on the radial distance from the point where the force is applied

FIGURE 9 Typical displacement field mapping experiment on the plasma membrane of a fibroblast. (*a*) Microscopic picture showing a region of the cell with one magnetic bead (M, radius 2.25 μm) and a number of nonmagnetic particles (1–9, radius 0.5 μm). (*b*) Graphic representation of the displacement field after a force pulse of 1-s duration. The bead sizes and positions are drawn to scale, while the bead deflections are enlarged by a factor of 10. The three non-numbered beads were also deflected, but the deflection amplitude could not be measured accurately enough since the images overlap, thus preventing the application of the particle tracking procedure. (*c*) Resulting distance dependence of the reduced radial component of bead deflection $u_r/\cos\theta$ as defined in Eq. 2. The dotted line is an optimal fit of Eq. 2 to the $u_r/\cos\theta$-versus-r plot giving the values of χ and μ^*. Closer inspection of Fig. 8 shows that the orientation of the deflection of the colloidal probes with respect to their angular position deviates from the theoretical prediction (Eqs. A5 and A6). The most likely explanation for these deviations is that the membrane is coupled to intracellular stress fibers, which is expected to lead to deviations from the isotropic displacement field. Moreover, the values of the deflections $u_r(\mathbf{r})$ show large scattering. This could also be caused by stress fibers, but could be due to variations in the degree of coupling of the colloidal probes to the integrin receptors of the membrane or differences in coupling of the receptors to the membrane-associated cytoskeleton.

if $r \ll R_c$ while $\mathbf{u}(r, \theta)$ decays exponentially if r is large compared to the screening length R_c.

To test the validity of such a screened displacement field we analyzed the distance-dependence of the displacement field by the displacement-field mapping technique (cf. Fig. 9). The displacement vector $\mathbf{u}(r, \theta)$ can be written in cylindrical coordinates (cf. Eq. A7). The radial component is given by

$$\frac{u_r(\mathbf{r})}{\cos\theta} = \frac{F_0}{2\pi\mu^*}\left\{\frac{3(1-\sigma)}{4}K_0(\kappa_1 r) - \frac{K_1(\kappa r)}{\kappa r}\right.$$
$$\left. + \left(\frac{1-\sigma}{2}\right)^{1/2}\frac{K_1(\kappa_1 r)}{\kappa r}\right\} \quad (2)$$

where $\mathbf{r}$ is the radius-vector from the center of the magnetic bead to the nonmagnetic colloidal probes, r is its absolute value, and θ is the angle between the force direction and $\mathbf{r}$. In Fig. 9 *c* the reduced radial displacement component $u_r/\cos\theta$ is plotted as a function of r.

By fitting the theoretical displacement field to the observed data one can estimate κ and thus R_c. This has been done in four cases yielding cutoff radii in the range of a few

micrometers. The fit shown in Fig. 9 *c* yields a value $\kappa \approx 0.15\ \mu\text{m}^{-1}$ corresponding to a cutoff radius $R_c \approx 7\ \mu$m and a surface shear modulus μ^* of $4 \cdot 10^{-3}$ Pa m. As $\kappa^2 = \chi/\mu^*$ the coupling constant is $\chi = 10^7$ Pa m^{-1}.

The surface shear modulus μ^* is also obtained by considering the absolute deflection of the magnetic bead in the direction of the magnetic field as a function of the force. The relationship between the deflection and the force is obtained by averaging the displacement $\mathbf{u}(R, \theta)$ at the boundary of the bead adhesion disk over all angles θ. At the present stage of analysis the radius is assumed to be about equal to the radius of the bead. Equation A2 yields

$$\langle u_x(R)\rangle = \frac{1}{2\pi}\int_0^{2\pi} u(R, \theta)d\theta$$
$$= \frac{F_{ex}}{4\pi\mu^*}[K_0(\kappa R) + (1-\sigma)K_0(\kappa_1 R)] \quad (3)$$

Comparison of Eq. 3 with Eq. A1 shows that the spring constant k of the equivalent circuit is related to the surface
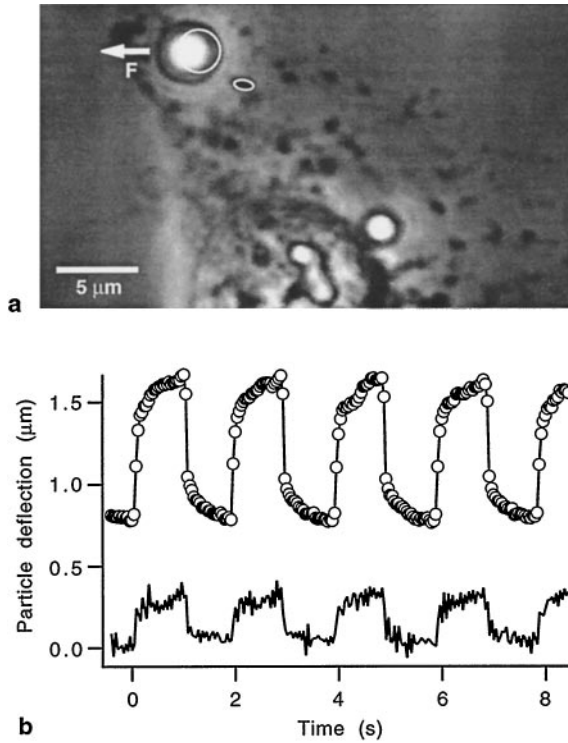
FIGURE 10   Demonstration of the penetration of the shear displacement field into the cell cytoplasm induced by displacement of the magnetic bead using cell vacuoles as markers. (*a*) Phase contrast image showing the magnetic bead (arrow pointing in the direction of the magnetic force) and some intracellular particles attributed to cell vacuoles in the deflected state. The initial position of the particles is marked by bright circular contours. Note that compartments further away from the magnetic bead, but at the same height as the one encircled, and those buried deeper in the cytoplasm do not move appreciably. (*b*) *Top trace:* sequence of creep response curves of magnetic bead following force pulses of duration $\Delta t = 1$ s. *Bottom trace:* Viscoelastic response curves of the marked cell vacuole.

shear modulus μ^* as

$$\mu^* = \frac{K_0(\kappa R) + (1 - \sigma)K_0(\kappa_1 R)}{4\pi} k \qquad (4)$$

Values of the surface shear moduli can be related to the spring constant k presented in Fig. 7 by assuming that the plate is incompressible ($\sigma \approx 0.5$) and that the screening length of the advancing lobes is about the same for all cells. With the value of κ obtained from the displacement field mapping experiments, the transformation factor $\{K_0(\kappa R) + (1 - \sigma)K_0(\kappa_1 R)\}/4\pi$ in Eq. 4 becomes 0.17 for a magnetic bead of the radius $R = 2.25$ μm. The average spring constant $k \approx 0.01$ Pa m (cf. Fig. 7) thus yields an average surface shear modulus $\mu^* \approx 2 \cdot 10^{-3}$ Pa m. Considering the large variability of the viscoelastic moduli of individual cells, this value agrees reasonably well with $\mu^* \approx 4 \cdot 10^{-3}$ Pa m obtained from the above analysis of the displacement field experiment.

The three-dimensional (3D) shear modulus of the cell envelope is related to μ by $\mu = \mu^*/h$. The thickness h of the composite membrane is certainly smaller than the cell lobe,

which is 1–2 μm. By assuming a value of $h \approx 0.1$ μm [as it was measured for neutrophils by Zhelev et al. (1994)] one obtains a 3D shear modulus of $\mu \approx 2 \cdot 10^4$ to $4 \cdot 10^4$ Pa.

It is important to experimentally estimate the values of the strain tensor to find out whether the linear approximation used for the calculations is valid. This can be done by calculating the measured relative displacements of the latex beads. This yields strains in the range of 2–5%, indicating that the measurements take place in the linear regime.

Evaluation of the viscous flow in terms of effective cytoplasmic viscosity

To relate the two-dimensional (2D) viscosity γ_0 of the equivalent circuit to the viscosity of the adhering cell lobe we assume that the magnetic bead is moving in a fluid membrane coupled to a solid surface through a viscous medium of thickness d_c. The situation is very similar to that of protein diffusion in fluid-supported membranes, which are separated from the solid surface by a lubricating film of viscosity η_c. This problem has been treated previously both theoretically and experimentally (Evans and Sackmann, 1988; Merkel et al., 1989). The viscous drag force on a disk embedded in the membrane and moving with velocity v is

$$F_d = 4\pi\eta_m\left[\frac{1}{4}\epsilon^2 + \epsilon\frac{K_1(\epsilon)}{K_0(\epsilon)}\right]v \qquad (5)$$

where $K_0(\epsilon)$ and $K_1(\epsilon)$ are modified Bessel functions. The dimensionless parameter ϵ is defined by $\epsilon = R(b_s/\eta_m)^{1/2}$. Here η_m is the 2D viscosity of the bilayer membrane, R is the radius of the disk which in our case is equal to the contact area between the magnetic bead and the membrane, and b_s is the friction coefficient of the coupling medium, which is related to the viscosity of the viscoelastic layer of thickness d_c by $b_s = \eta_c/d_c$. For large values of ϵ (in practice, for $\epsilon > 1$), the second term on the right side of Eq. 5 can be neglected. The drag force in this limit does not depend on the membrane viscosity and is $F_d = \pi R^2 d_c^{-1}\eta_c v$. The 2D viscosity of membranes is of the order of $\eta_m = 10^{-9}$ N s/m (Merkel et al., 1989), d_c is ~2 μm, and η_c is typically of the order of 200 Pa s (Bausch et al., 1998, submitted for publication). Therefore, $\epsilon \approx 10^2$ and the above approximation is well fulfilled in our case. Consequently, the effective viscosity γ_0 of the equivalent circuit is related to the friction coefficient of the coupling medium (the cytoplasm) by the obvious relation: $b_s = \gamma_0/\pi R^2$.

The viscosity γ_0 obtained from the slope of the viscous flow regime of the creep response curve is $\gamma_0 = 0.03$ Pa s m. By assuming that the radius of the contact area of the bead on the membrane is about equal to the bead radius ($R = 2.25$ μm) one obtains for the friction coefficient of the cytoplasm a value of $b_s \approx 2 \cdot 10^9$ Pa s/m. By assuming $d_c \approx 2$ μm our estimation yields $\eta_c \approx 4 \cdot 10^3$ Pa s.

DISCUSSION

The magnetic bead rheometer designed in the present work allows generation of forces in the nanonewton range, which are strong enough to enable local measurements of viscoelastic parameters of cell envelopes (comprising the lipid/protein bilayer and the associated actin cortex). By application of the high-resolution particle tracking technique bead deflections may be measured with at least 10 nm lateral resolution and a time resolution of 0.04 s. The viscoelastic response is linear at least up to forces of 2000 pN, corresponding to maximum displacement amplitudes of 1 μm. Most measurements, with the exception of some of the displacement field experiments, were performed at 500-1000 pN, corresponding to displacements of 250–500 nm.

The creep response curves of the cells are analyzed in terms of the equivalent circuit because this model can be most easily adapted to the observed creep response curves in a model-free manner. The relationships between the viscoelastic parameters of the equivalent circuit and the viscoelastic moduli of the cell surface are, however, model-dependent and it is therefore most convenient to analyze measurements first in terms of the equivalent circuit.

Our displacement field mapping experiments show that the elastic displacement of the cell surface generated by local tangential forces is screened at lateral distances of a few micrometers from the point of attack. Strong screening of the elastic deformation has also been established recently in the cytoplasm by similar displacement field mapping experiments (Bausch et al., 1998, submitted for publication; unpublished data of this laboratory). This screening of the elastic deformation of the membrane and the cytoskeleton is an important condition for the local measurement of viscoelastic parameters on cell surfaces. However, local measurements are important for at least two reasons. First, they allow the study of viscoelastic properties of closed shells by restricting to the analysis of local deformations. Second, cell envelopes generally exhibit heterogeneous lateral organizations, and the elastic deformation may also be anisotropic due to coupling of various cytoskeletal elements including stress fibers to the actin cortex.

The absolute values for the shear modulus and the viscosity obtained by modeling the cell lobe as two elastic sheets coupled by a viscoelastic gel are certainly rough estimates. However, the values agree rather well with data obtained by other techniques. In our study an average 3D shear modulus of $\mu \approx 2 \cdot 10^4$ to $4 \cdot 10^4$ Pa is obtained. This value is in acceptable agreement with the AFM measurements. Thus, AFM measurements performed on human platelets by Radmacher et al. (1996) yield bulk moduli of 1–50 kPa, while in chicken cardiocytes the elastic moduli range from 10 to 200 kPa. The latter value is measured on top of stress fibers (Hofmann et al., 1997).

Our results are in contrast to findings of Wang et al. (1993), who used a twisting rheometer to measure the viscoelastic properties of bovine capillary endothelial cells. Apparent Young's moduli of ~8 Pa and viscosities of 5–10

Pas were obtained, about four orders of magnitude smaller than our values. The discrepancy may be due to the way the deformation is applied: we apply a real shear force, whereas in the experiments of Wang et al. (1993) a twisting force is applied. This also makes it difficult to compare the absolute values of the applied stresses. Assuming an approximate radius of the adhesion area of the bead of 1–2.25 μm, we estimate applied stresses of ~$300-60$ Nm^{-2}, while in the measurements of Wang et al. the stresses are only 3 Nm^{-2}. In separate experiments we found that application of such small forces leads to detectable deflections only if the beads are attached to the extracellular matrix. Furthermore, the strain hardening reported by these authors could not be reproduced in our studies. As can be seen in Fig. 10, saturation effects were observed only for forces exceeding 2000 pN.

Our analysis yields an average value for the cytoplasmic viscosity of $2 \cdot 10^3$ Pa s. Sato et al. (1984) found for the cytoplasmic viscosity of the axoplasm of squid axon a value of 10^4-10^5 Pa s, while Valberg and Butler (1987) and Valberg and Feldman (1987) using twisting rheometry have found values ranging from 250 to 2800 Pa s inside macrophages, in good agreement with our results.

The viscosity obtained by our method should be compared with the value measured by the micropipette aspiration technique developed by Evans (1995) which was applied by Tsai et al. to human neutrophils (1994). In this case the viscosity is obtained from the speed of penetration of the cell into the pipette at a constant suction pressure. Typical values found are of the order of 100 Pa s, which are an order of magnitude smaller than our value. This may be due to the fact that our measurements are done on the rather flat advancing lobe of the fibroblast, which may exhibit a much higher viscosity than the whole cell body of blood cells.

It should be also noted that the origin of the viscous flow regime is not understood yet. In the framework of the present model it would be determined by the rate of decoupling (fracture) of the connections between the membrane-associated actin cortex and the intracellular cytoskeleton. It could, however, be determined equally well by the fracture of lateral cross-links within the actin cortex. A decision between these two possibilities cannot be made on the basis of the present experiments.

An intriguing finding of the current analysis is that the displacement field seems to be anisotropic, as is demonstrated by the large deviations of the direction of deflection of the colloidal probes from the direction of an isotropic displacement field. This may be a consequence of the coupling of the actin cortex to local stress fibers. By improving the technique of selective coupling of smaller probe beads to membrane receptors, the displacement field mapping technique could probe local elastic anisotropies of the plasma membrane and the underlying cytoskeleton.

The magnetic bead technique provides a versatile tool for cell rheometry. By deposition of several beads it allows simultaneous measurements at different sites on the cell surface (cf. Fig. 3 *a*). The technique can be simultaneously

applied to the cell surface and the cytoplasm. As it is essentially a nonperturbing technique creep, response curves can be recorded repeatedly. This allows detection of temporal changes of the local viscoelasticity. It may thus also be applied to evaluate local changes of the cytoskeletal structure (e.g., the formation of stress fibers) caused by local mechanical agitations or by the binding of integrins. Such local modifications of the cytoskeleton were recently reported for endothelial cells by Chicurel et al. (1998). Evidence was provided that coupling of colloidal beads to integrins leads to a local reorganization of the actin cortex, resulting in an increase of the messenger RNA concentration near the focal adhesion site 20 min after integrin binding.

The above considerations suggest that magnetic bead rheometry is a promising new technique to gain insight into such biochemically induced changes of the local constitution of the cell cytoskeleton.

APPENDIX

Elastic deformations of juxtaposed coupled membranes by local tangential force

The cell membrane, consisting of the lipid bilayer attached to the actin cortex, is represented by a thin elastic plate supported by a viscoelastic substrate. The lobe shape makes it possible to assume that its top membrane is flat. The bottom membrane is considered as rigid and fixed to the solid substrate. A basic assumption of the present model is that the actin cortex is coupled to the bulk cytoskeleton consisting of microtubules, intermediate, and actin filaments. To consider the effect of this gel on the membrane deformation we adopt the simplified mechanical model of the cell lobe displayed in Fig. 11. The bulk cytoskeleton is assumed to consist of pre-stressed and unstressed compartments. The former consist of the stress fibers, which either penetrate the whole thickness of the lobe connecting the top and the bottom membranes (cf. Fig. 11, b and c; filaments numbered 1), or connect the top membrane to a stressed region of the network, which is attached to the bottom membrane by another stress fiber (cf. Fig. 11, b and c; fibers marked by number 2). Assume that the lobe possesses n_{st} such stress fibers per unit area and that they exhibit an average tension T. Besides the pre-stressed fibers, the bulk cytoskeleton
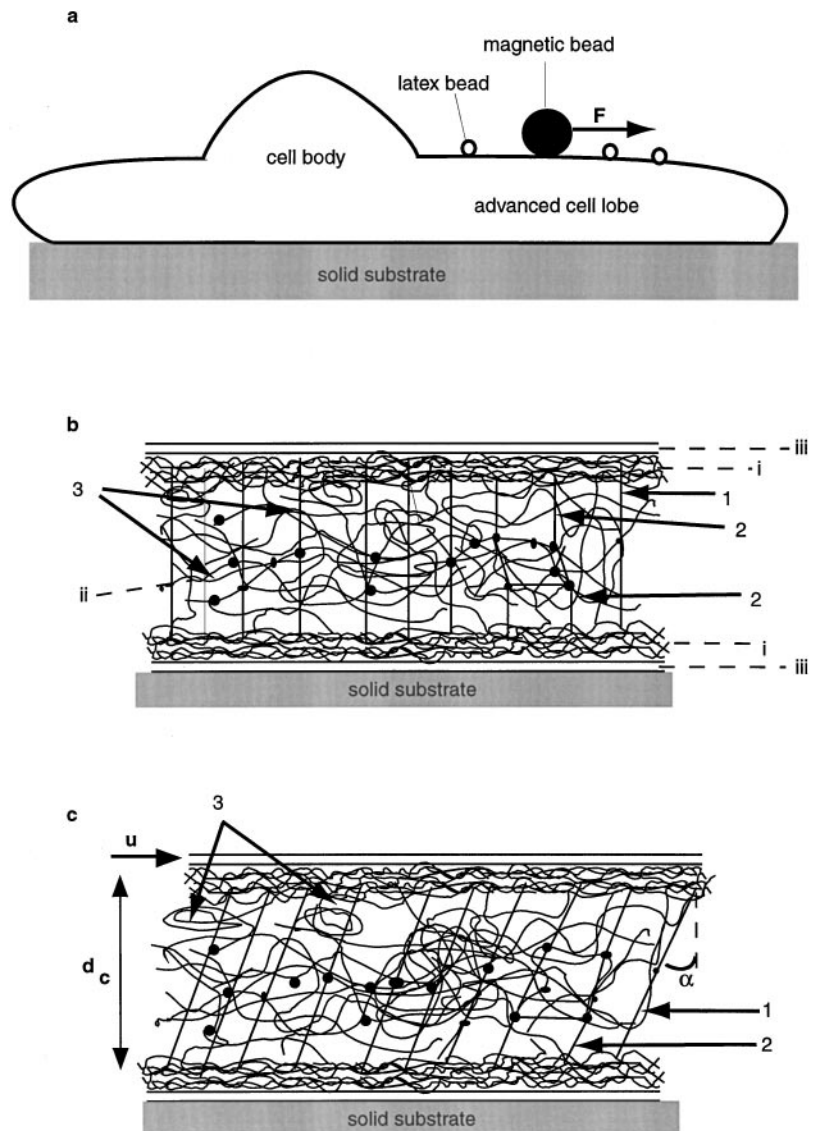

FIGURE 11 Schematic view of the mechanical model of the cell lobe. (a) General view of the mouse fibroblast. The numbers indicate (1) the solid substrate, (2) the cell body, (3) the advanced cell lobe, (4) the nonmagnetic, and (5) the magnetic beads coupled to the top membrane of the lobe. (b) Schematic view of the structure of the undeformed lobe. (i) Actin cortexes of the top and the bottom membranes, (ii) bulk cytoskeleton, (iii) lipid bilayers, (iiii) solid substrate. The Arabic numbers indicate (1) the stress fibers penetrating through the whole lobe, (2) stress fibers connected with the prestressed parts of the bulk cytoskeleton, and (3) unstressed components of the cytoskeleton connected with the actin cortex. (c) Shear displacement of the complex membrane/actin cortex causes tilting of the stressed fibers by the angle $\alpha \approx u/d_c$ and stretching of those unstressed parts of the cytoskeleton that are cross-linked to the actin cortex.

may contain unstressed parts of the network coupled to the actin cortex (cf. Fig. 11, *b* and *c*; fibers number 3). An in-plane displacement of the cortex $\mathbf{u} = (u_x, u_y)$ is followed by tilting of the stress fibers in the pre-stressed parts of the cytoskeleton. It causes bending of the stiff microtubules and intermediate filaments and stretching of wrinkles and meshes of the unstressed parts of the cytoskeleton. Therefore, the unstressed parts of the cytoskeleton can be characterized by the number density n_{un} of attachments of these components to the actin cortex and by an average spring constant k_{un}. Under a lateral membrane displacement u both mechanisms give rise to a restoring force $|\mathbf{F}_{rest}| = S(Tn_{st} \tan \alpha + k_{un}n_{un}|\mathbf{u}|)$, where S is the membrane area. The first term describes the contribution of the pre-stressed and the second of the unstressed cytoskeletal components. Making use of the relation $\tan \alpha \approx u/H$ one finds

$$\mathbf{F}_{rest} = -S\left(\frac{Tn_{st}}{d_c} + k_{un}n_{un}\right)\mathbf{u} \qquad (A1)$$

One defines the coupling constant χ as $\mathbf{F}_{rest} = -S\chi\mathbf{u}$ where

$$\chi = k_{un}n_{un} + \frac{Tn_{st}}{d_c} \qquad (A2)$$

In a real cell the mechanism of formation of the restoring force can be more complicated. Therefore, one should consider χ as a phenomenological parameter that has the dimension of a spring constant per unit membrane area.

The displacement field generated by a local tangential force on the top membrane has been calculated by Boulbitch (1998, submitted for publication) and the theory is summarized below.

The equation of the mechanical equilibrium of a 3D body is well-known (Landau and Lifshitz, 1959). To transform it to the case of a thin plate, an averaging procedure (over the direction perpendicular to the plane) has to be performed (Muschelishvili, 1963). This allows expression of the equation of equilibrium in terms of a membrane shear modulus μ^* obtained by integrating the shear modulus over the membrane thickness h: $\mu^* = \mu h$. Taking into account the restoring force mentioned above, one obtains the following equation of the mechanical equilibrium of the composite membrane:

$$\Delta\mathbf{u} + \frac{1 + \sigma}{1 - \sigma} \text{grad div } \mathbf{u} - \kappa^2\mathbf{u} = -\frac{\mathbf{F}}{\mu^*} \qquad (A3)$$

where $\kappa^2 = \chi/\mu^*$. Here κ^{-1} is a length scale. As will become evident below, $R_c = \kappa^{-1} = (\mu^*/\chi)^{1/2}$ is a cutoff radius that accounts for the screening of the displacement field by the cytoskeleton. By considering Eq. A2 one obtains

$$R_c = \left(\frac{\mu^* d_c}{k_{un}n_{un}d_c + Tn_{st}}\right)^{1/2} \qquad (A4)$$

In the case of a thin lobe ($d_c \ll T/k_{un}$) one finds $R_c \approx (d_c\mu^*/Tn_{st})^{1/2}$. In the opposite case $R_c \approx (\mu^*/k_{un}n_{un})^{1/2}$.

If the cutoff radius is much larger than the radius of the magnetic bead R ($R_c \gg R$) one can assume that the force is point like $\mathbf{F} = F_0\delta(\mathbf{r})$ where F_0 is the absolute value of the force acting on the magnetic bead along the x axis. The displacement field for the local tangential force is given by the following expressions:

$$u_x(\mathbf{r}) = \frac{F_0}{2\pi\mu^*}\left\{\frac{1}{2}K_0(\kappa r) + \frac{1 - \sigma}{2}K_0(\kappa_1 r) - \cos 2\theta\left[\frac{K_1(\kappa r)}{\kappa r}\right.\right.$$
$$\left.\left. - \sqrt{\frac{1 - \sigma}{2}}\frac{K_1(\kappa_1 r)}{\kappa r} + \frac{1}{2}K_0(\kappa r) - \frac{1 - \sigma}{4}K_0(\kappa_1 r)\right]\right\} \qquad (A5)$$
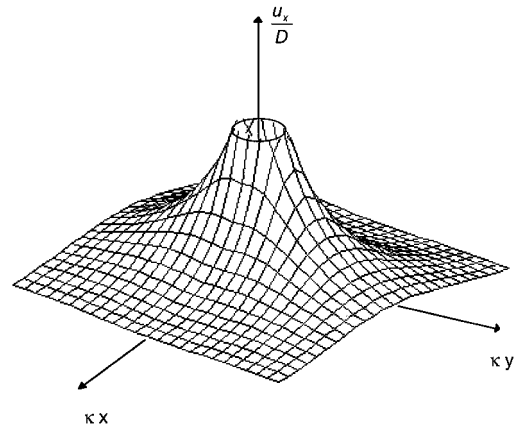

FIGURE 12 Dependence of the displacement vector component $u_x(\mathbf{r})$ on coordinates as described by Eq. A5. The normalizing factor is $D = 4\pi\mu^*/F_0$.

$$u_y(\mathbf{r}) = -\frac{F_0\sin 2\theta}{2\pi\mu^*}\left\{\frac{K_1(\kappa r)}{\kappa r} - \sqrt{\frac{1 - \sigma}{2}}\frac{K_1(\kappa_1 r)}{\kappa r}\right.$$
$$\left. + \frac{1}{2}K_0(\kappa r) - \frac{1 - \sigma}{4}K_0(\kappa_1 r)\right\} \qquad (A6)$$

where K_0 and K_1 are modified Bessel functions of the second kind (and order zero and one, respectively) and $\kappa_1 = [(1 - \sigma)/2]^{1/2}\kappa$. Note that for the limiting case $R \to \infty$ the equations (A5–A6) describe the elastic deformation of a single thin plate, the displacement field exhibiting the well-known logarithmic behavior usual for the flat theory of elasticity (Muschelishvili, 1963). The component u_x of the displacement as a function of coordinates is shown in Fig. 12.

The displacement components can be expressed in cylindrical coordinates. Introducing the unit vector $\mathbf{n} = (\cos \theta, \sin \theta)$ directed along the radius-vector $\mathbf{r}$ the radial component of the displacement vector $\mathbf{u}$: $u_r = (\mathbf{u} \cdot \mathbf{n})$ is given by

$$u_r(\mathbf{r}) = \frac{F_0}{2\pi\mu^*}\cos\theta\left\{\frac{3(1 - \sigma)}{4}K_0(\kappa_1 r) - \frac{K_1(\kappa r)}{\kappa r}\right.$$
$$\left. + \sqrt{\frac{1 - \sigma}{2}}\frac{K_1(\kappa_1 r)}{\kappa r}\right\} \qquad (A7)$$

which gives Eq. 2 above.

REFERENCES

Chicurel, M. E., R. H. Singer, C. J. Meyer, and D. E. Ingber. 1998. Integrin binding and mechanical tension induce movement of mRNA and ribosomes to focal adhesions. *Nature.* 392:730–733.

Choquet, D., D. P. Felsenfeld, and M. P. Sheetz. 1997. Extracellular matrix rigidity causes strengthening of integrin-cytoskeleton linkages. *Cell.* 88:39–48.

Evans, E. 1995. Physical action in biological adhesion. *In* Handbook of biological Physics, Vol 1. R. Lipowsky and E. Sackmann, editors. Elsevier, Amsterdam.

Evans, E., and E. Sackmann. 1988. Translational and rotational drag coefficients for a disk moving in a liquid membrane associated with a rigid substrate. *J. Fluid Mech.* 194:553–561.

Forgacs, G. 1996. Biological specificity and measurable physical properties of cell surface receptors and their possible role in signal transduction through the cytoskeleton. *Biochem. Cell Biol.* 73:317–326.

Fung, Y. C. 1993. Biomechanics: Mechanical Properties of Living Tissues. Springer Verlag, New York.

Hofmann, U. G., C. Rotsch, W. J. Parak, and M. Radmacher. 1997. Investigating the cytoskeleton of chicken cardiocytes with the atomic force microscope. *J. Struct. Biol.* 119:84–91.

Ingber, D. E. 1997. Tensegrity: the architectural basis of cellular mechanotransduction. *Annu. Rev. Physiol.* 59:575–599.

Landau, L. D., and E. M. Lifshitz. 1959. Theory of Elasticity. Pergamon Press, Oxford.

Merkel, R., E. Sackmann, and E. Evans. 1989. Molecular friction and epitactic coupling between monolayers in supported bilayers. *J. Phys. France.* 50:1535–1555.

Miyamoto, S., S. K. Akiyama, and K. M. Yamada. 1995. Synergistic roles for receptor occupancy and aggregation in integrin transmembrane function. *Science.* 267:883–885.

Muschelishvili, N. J. 1963. Some Basic Problems of the Mathematical Theory of Elasticity. Noordhoff Verlag, Groningen.

Pasternak, C., S. Wong, and E. L. Elson. 1995. Mechanical function of dystrophin in muscle cells. *J. Cell Biol.* 128:355–361.

Radmacher, M., M. Fritz, C. M. Kacher, J. P. Cleveland, and P. K. Hansma. 1996. Measuring the viscoelastic properties of human platelets with the atomic force microscope. *Biophys. J.* 70:556–567.

Sato, M., T. Z. Wong, D. T. Brown, and R. D. Allen. 1984. Rheological properties of living cytoplasm: a. Preliminary investigation of squid axoplasm (*Loligo pealei*). *Cell Motil.* 4:7–23.

Schmidt, F. G., F. Ziemann, and E. Sackmann. 1996. Shear field mapping in actin networks by using magnetic tweezers. *Eur. Biophys. J.* 24:348–353.

Simson, R., E. Wallraff, J. Faix, J. Niewöhner, G. Gerisch, and E. Sackmann. 1998. Membrane bending modulus and adhesion energy of wild-type and mutant cells of *Dictyostelium* lacking talin or cortexillins. *Biophys. J.* 74:514–522.

Tsai, M. A., R. S. Frank, and R. E. Waugh. 1994. Passive mechanical behavior of human neutrophils: effect of cytochalasin B. *Biophys. J.* 66:2166–2172.

Valberg, P. A., and J. P. Butler. 1987. Magnetic particle motions within living cells. Physical theory and techniques. *Biophys. J.* 52:537–550.

Valberg, P. A., and H. A. Feldman. 1987. Magnetic particle motions within living cells. Measurement of cytoplasmic viscosity and motile assay. *Biophys. J.* 52:551–69.

Wang, N., J. P. Butler, and D. E. Ingber. 1993. Mechanotransduction across the cell surface and through the cytoskeleton. *Science.* 260:1124–1127.

Zhelev, D. V., D. Needham, and R. M. Hochmuth. 1994. Role of the membrane cortex in neutrophil deformation in small pipettes. *Biophys. J.* 67:696–705.

Ziemann, F., J. Rädler, and E. Sackmann. 1994. Local measurements of viscoelastic moduli of entangled actin networks using an oscillating magnetic bead microrheometer. *Biophys. J.* 66:2210–2216.